ORIGINAL

Performance assessment of PVT-air collector with V-groove absorber: A theoretical and experimental analysis

Sourav Diwania[1] · Anwar S. Siddiqui[1] · Sanjay Agrawal[2] · Rajeev Kumar[1,3] (ID)

Abstract

In this paper, the performance of a PVT (photovoltaic thermal) air collector with V-groove absorber in the air channel is theoretically and experimentally examined under different climate conditions of Ghaziabad city, India, in summer, June 2019. A low power brushless DC fan is fixed at the input of the air-channel to ensure the circulation of air through the V-groove. The energy balance equation is developed with the matrix-inversion method to estimate the PV (photovoltaic) cell and air output temperatures. The theoretical results obtained using mathematical modeling has been compared with that of the real-time experimental results. The electrical, thermal, and overall efficiencies for the theoretical and experimental studies are found in the range of 10.39–10.26%, 41.78–41.57%, and 52.17–51.81%, respectively. It has been observed that the theoretical results are coherent with experimental results for the proposed model achieving an accuracy of 98.98%, 99.43%, and 99.31% for electrical, thermal, and overall efficiencies, respectively.

Nomenclature

A_c	Collector area (m^2)
H_t	Collector top loss coefficient (W/m^2 ^{o}C)
H_b	Collector back loss coefficient (W/m^2 ^{o}C)
T_c	Cell temperature (^{o}C)
d	Channel depth (m)
D_c	Equivalence diameter of channel (m)
Ex_{in}	Exergy input
Ex_{out}	Exergy output
T_f	Fluid Temperature (^{o}C)
m	Mass flow rate (kg/s)
A_m	Module area (m^2)
N_u	Nusselt number
P_r	Prandtl number
Re	Reynolds number
I	Solar radiation (W/m^2)
C_f	Specific heat (J/kg ^{o}C)
T_{in}	Temperature at the channel inlet (^{o}C)
T_{out}	Temperature at the channel output (^{o}C)
T_{sun}	Temperature of the sun (^{o}C)
k	Thermal conductivity (W/m ^{o}C)
Q_t	Usable heat (W)
W	Width of the channel (m)

Abbreviations

PV	Photovoltaic
PVT	Photovoltaic Thermal
HTC	Heat transfer coefficients

Greek symbols

α	Absorption coefficient
ρ	Air density (kg/m^3)
ϵ_p	Emissivity of PV
η_{ele}	Electrical efficiency,%
η_{Ex}	Exergy efficiency, %
$\eta_{overall}$	Overall efficiency, %
σ	Stefan Boltzman constant
β_0	Temperature coefficient of efficiency
μ	Viscosity (kg/ms)
η_{th}	Thermal efficiency, %
τ	Transmission coefficient

✉ Rajeev Kumar
rajeev.rakshit@gmail.com

1 Department of Electrical Engineering, Jamia Millia Islamia, New Delhi, India

2 School of Engineering and Technology, IGNOU, New Delhi, India

3 Department of Electrical and Electronics Engineering, Krishna Institute of Engineering and Technology, Ghaziabad, India

Subscripts

a	ambient
b	backplate
f	fluid
p	photovoltaic
r	radiative
s	sky
w	wind

1 Introduction

The growth trajectory of any developing country cannot be projected without studying the rise in its electricity requirements. India's story of development is no more different, considering the exponential surge in power requirement over the last decade. However, the national grid infrastructure has struggled to keep pace with power generation. India is working on all fronts to reduce its reliance on traditional fossil-based fuels, replacing them with renewable energy to encounter the energy challenges.

With the upsurge in power demand over the coming decade and rapid installation of renewable power sources such as wind and solar, India's existing grid network will require a significant expansion in a very short duration. The development in the renewable energy sector ensures reduced carbon emission, uninterrupted energy supply, job opportunities, clean energy production, and electricity in rural areas. In India, exponential growth has been observed in the generation of power using solar photovoltaic technology and reached up to 31.5 GW, which is 8.73% of the overall installed capacity as estimated at the end of June 2019 [1]. The state-wise allocation of solar PV installed capacity until September 2019 is shown in Fig. 1. Around 73% of rooftop solar installation is meant for a commercial and industrial segment, while the rest of 27% is for residential purposes [2]. The overall installed capacity of solar PV rooftop in India at the end of 2019 is 5252 MW.

Tomar et al. [3] experimentally verified the thermo-electrical performance of five various types of PV-modules, i.e., monocrystalline silicon (m-Si), polycrystalline (p-Si), amorphous thin film (a-Si), cadmium telluride thin film (CdTe), and copper indium gallium de-selenide (CIGS) integrated with a thermal management system. Monocrystalline silicon holds the maximum market share as it offers better performance compared to various silicon-based PV technologies. The higher cost of m-Si opens the path for the commercialization of p-Si and the latest thin-film technologies. Among all the latest thin-film technologies, amorphous thin film (a-Si) technology gains significant popularity due to its low cost and its effectiveness in low-temperature regions [4].

Photovoltaic technology uses sunlight to generate electrical energy, thus eliminating the dependency on conventional energy sources. In solar thermal systems, the solar collector is an elementary element that converts the sunlight into thermal energy. The high operating temperature of the PV-module causes structural damages and reduced electrical conversion efficiency [5]. Hence, PV-modules must be coupled with a thermal management system to maintain the working temperature within the permissible limits. Previous research shows that the heat extracted using the PV-module can be reused for various domestic and commercial purposes. Thus, the hybrid PVT technology consisting of solar PV and thermal management system is used to improve the electrical output by drawing the heat from the module using air/water as a coolant in the channel below the PV-module [6]. The PVT collector is widely used for converting solar energy into thermal and electrical energy simultaneously, as shown in Fig. 2. The hybrid system is highly efficient than the solar PV-system and requires less space, material, and cost of installation.

The working temperature is reduced using both natural and forced circulation of fluid (air/water) via the channel below the PV-module. This helps in the cooling of the PV-module, resulting in increased electrical efficiency (η_{el}) [7, 8].

Recently, many studies have been carried out to test the effect of glazing on the efficiency of the PVT-system, as shown in Table 1. Kazemian et al. [9] experimentally verified the impact of the additional glass cover and different working fluid (water, ethylene glycol/water, and pure ethylene glycol) on the efficiency of glazed and unglazed PVT-system. It is found that the unglazed PVT-system is preferred when electrical efficiency is the prime interest, while the glazed PVT-system has opted when higher overall efficiency is desired. The impact of solar cell emissivity on the η_{th} of the PVT-system has been investigated by Lammle et al. [10] by using a selective coating on the cell. A significant reduction in heat losses has been observed by using the selective coating over the solar cell.

Air as a cooling fluid in the channel ensures simplicity in the design, along with greater safety. Still, at the same time, it offers low thermal conductivity and specific heat, which results in low η_{th}. That's why most of the researchers diverted their studies towards the use of water along with nano-fluids as a heat transfer medium. The inclusion of nanoparticles with the base fluid in the channel raises the thermal efficiency of the PVT-system. A number of research works are performed to examine the effect of size, volume fraction, and a suitable concentration of nanoparticles with base fluid. Abbas et al. [13] presented a detailed analysis to show the effect of nanoparticles upon the PVT-system's efficiency. It is observed that the organic fluids offer better thermal conductivity concerning water when used as a base fluid. A comparative study on PVT, PVT with nano-fluid, and PVT-PCM system have been conducted by Sardarabadi et al. [14]. The outcomes showed that η_{Ex} of the PVT with nano-fluid is better as compared to other PVT- systems. Ali et al. [15] examined the impact of carbon-

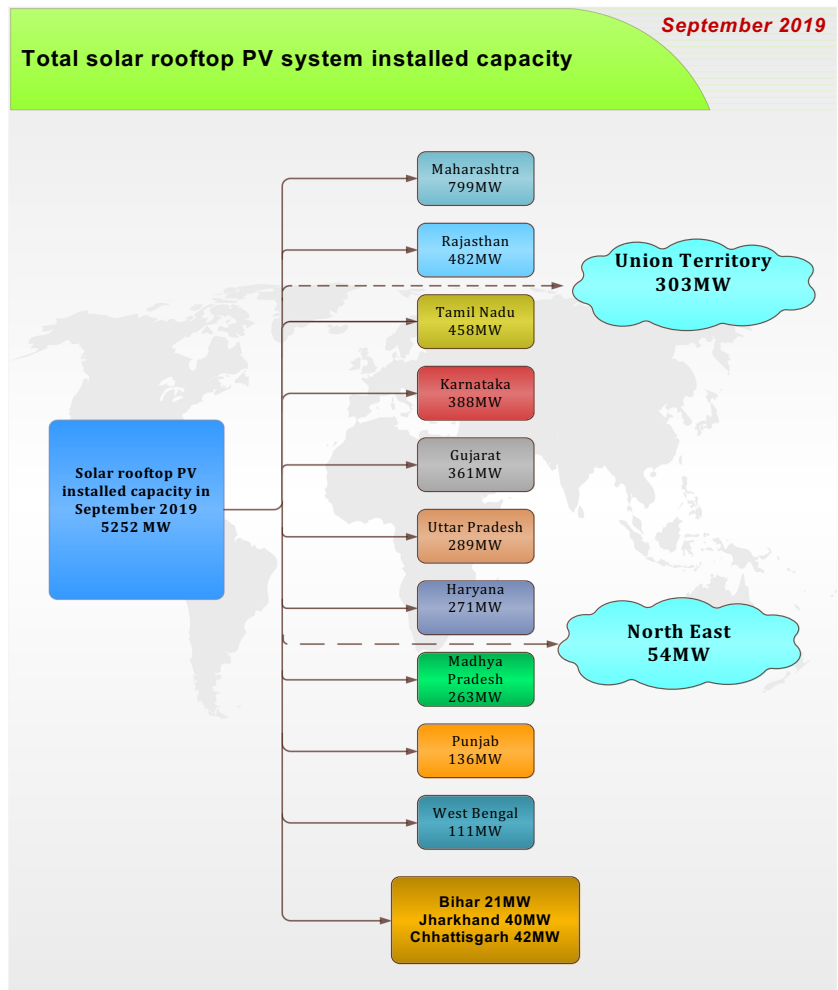**Fig. 1** State-wise allocation of solar rooftop PV-system in India [2]
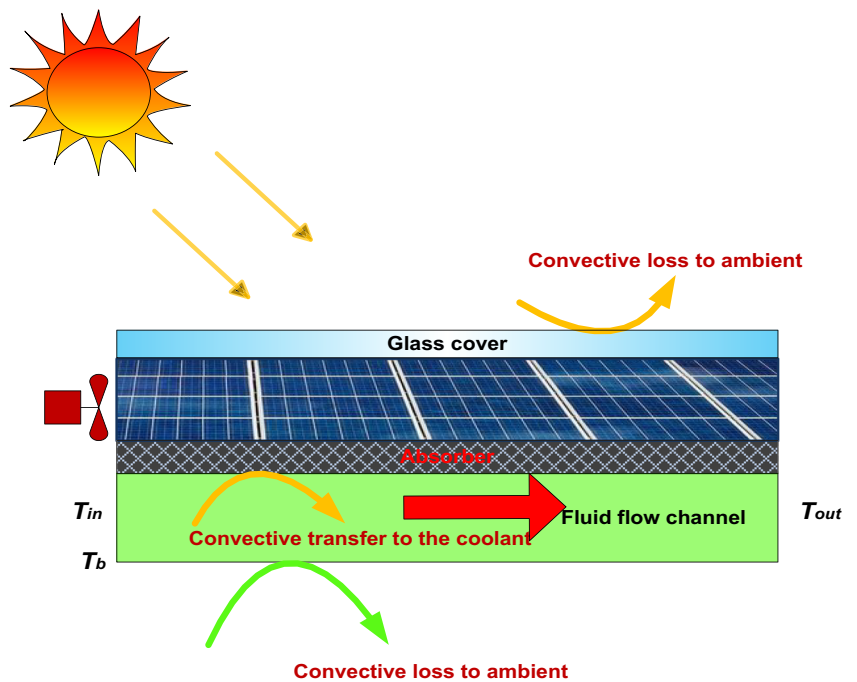

Fig. 2 Typical PVT air-collector

Table 1 Impact of glazing on the PVT-system

Author	Year	Type of coolant	Electrical efficiency (η_{el})		Thermal efficiency (η_{th})	
			Glazed	Unglazed	Glazed	Unglazed
Rejeb et al.[11]	2015	water	13.90%	16.00%	58.00%	40.00%
Yazdanifard et al. [12]	2016	water	11.50%	10.50%	57.00%	67.00%
Kazemian et al. [9]	2018	water	13.15%	14.35%	70.89%	63.37%
		water/ethylene glycol	11.36%	14.13%	68.27%	59.95%
		pure ethylene glycol	10.20%	13.16%	53.75%	44.68%

based nanoparticles, especially SiC, on the η_{th} of the PVT-system.

Singh et al. [16] formulated a mathematical model of the PVT-system considering the effect of the absorber plate shape factor and mass-flow rate. From the analysis, it has been concluded that the absorber plate shape factor is an important factor that influences the efficiency of the PVT-system. Jones et al. [17] presented a novel mathematical model on a two-node approach to estimate the thermal and electrical efficiencies of the PVT-collector.

Exergy analysis is a useful technique for estimating the efficiency of PVT-systems as it helps in suppressing the inefficiencies in the system and enables to estimate the amount of loss in the system. Fudholi et al. [18] investigated the exergetic performance of ∇- groove absorber installed in the channel of the PVT-system. Salem et al. [19] presented an experimental description of the hybrid PVT-system with straight and helical aluminium plates for cooling. The average η_{Ex} of the hybrid system was 11.1% and 13.5% for experimental and theoretical studies, respectively. Tadesse [20] experimentally examined the PVT air-collector with a V-groove absorber in a channel below the module. The performance of the PVT-collector is significantly enhanced by using V-groove in the channel. A comparison of the present work with the existing state-of-art is shown in Table 2.

Dust and pollution significantly affect both the productivity and conversion efficiency of a PV module. Accumulation of the dust on the upper surface of PV modules results in energy loss and damage of the upper layer [31]. Dust includes bird droppings, sand, microfiber, hair, and plant products. The dust accumulation on the upper surface of the PV module is a function of the physical and chemical properties of dust particles such as size, weight, and shape. Ecological factors such as temperature, moisture, wind direction, wind speed, and rainfall also affect the dust deposition to a large extent [32]. The optical, thermal, and electrical characteristics of the PV module are also affected by the amount of dust deposition. Molki [33] conducted an experimental study to investigate the impact of the deposition of ground clay (bentonite) over the performance and efficiency of the PV module. The

outcomes show that the overall efficiency decays with a rise in the deposition of bentonite. Kazem et al. [34] investigate the effect of sand, ash, silica, and calcium carbonate deposition on the performance of the PV module. The study reveals; maximum loss in PV voltage occurs with the deposition of ash over the surface of the PV module.

Dust deposition not only affects the thermal and electrical performance of the PV module but also reduces its lifetime. Therefore, the cleaning of dust is necessary for the performance and lifetime enhancements of the PV modules. There are various methods of cleaning, such as natural cleaning (rainfall, wind), manual cleaning (washing), and automated cleaning. In the present work, manual cleaning (water and soft cloth) has been opted to clean the PV module.

1.1 Main contribution

- In this study, V-groove is inserted in the PVT air collector channel to raise the thermal conductivity.
- The efficiency of the PVT air-collector is evaluated in terms of η_{th}, η_{el}, and η_T.
- The energy balance equation has been derived with the help of the matrix inversion method to predict the PV and air output temperatures.
- The exergy efficiency of the proposed system is analyzed based on real-time data.
- The experimental results are compared with theoretical results based on mathematical modeling using the same weather conditions to validate the proposed model.

The Section 1 includes the latest research conducted in the PVT air-collector accompanied by the impact of channel modifications on the PVT-system performance. The Section 2 incorporates the mathematical modeling of the proposed system with the energy balance equation. In the Section 3, the specifications of the PVT-module have been discussed in detail. In the Section 4, the experimental and theoretical results have been analyzed. The Section 5 concludes the paper with justified references.

Table 2 Comparison of the present work with current state-of-art

Author	Year	Description of the PVT-system	Exergy efficiency, η_{Ex} (%)	
			Experimental	Theoretical
Fudholi et al. [18]	2018	PVT air-collector with ∇-groove absorber installed in the channel	12.66	12.91
Salem et al. [19]	2017	PVT air-collector with aluminum plates in the channel	11.1	13.5
Khanjari et al. [21]	2016	PVT water collector with silver as a nano-fluid	15	-
Hazami et al. [22]	2016	PVT air-collector system	14.8	-
Jahromi et al. [23]	2015	PVT water collector	9.6	9.7
Ibrahim et al. [24]	2014	PVT water collector	12.0	14.0
Gholampour and Ameri [25]	2016	Flat plate PVT air collector	8.66	-
Wu et al. [26]	2011	Heat pipe PVT hybrid system	10.26	-
Sarhaddi et al. [27]	2010	Flat plate air-based PVT collector	-	10.75
Khaki et al. [28]	2017	BIPV/T system	-	Unglazed: 10.81 Glazed: 10.75
Agrawal and Tiwari [29]	2011	Hybrid micro-channel PVT air- collector	9.38	18.03
Das et al. [30]	2018	PVT air-collector with the inclusion of thermal contact resistance	8.89	10.03
Present Study	2020	PVT air-collector with V-groove absorber	12.70	12.94

2 Mathematical modeling

The energy balance equation to predict the PV and air output temperature in the proposed system has been developed based on the following assumptions:

1) The system is assumed in a steady-state.
2) The specific heat of the fluid remains invariable in the channel.
3) The convective heat transfer coefficients across the air channel, and the air remains constant and equal.
4) Ohmic losses from the PV-module remain constant.
5) The useful heat gained by the fluid remains constant throughout the channel length.

The cross-sectional view of the PVT air-collector with V-groove absorber in the air channel is shown in Fig. 3.

The energy balance equation can be derived as:

For PV-module

$$\alpha\tau I = H_t(T_p - T_a) + h_A(T_p - T_f) + h_{rpb}(T_p - T_b) + \eta_{pv}I + Q_t \tag{1}$$

Energy balance equation for the channel

$$mC_f(T_o - T_i) = h_A(T_p - T_f) + h_B(T_b - T_f) + Q_t \tag{2}$$

At the back surface

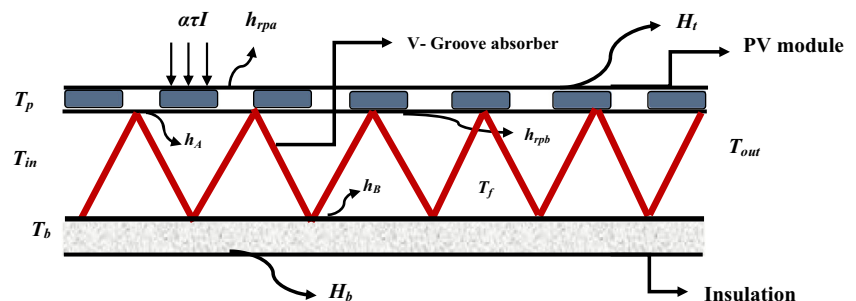$$h_{rpb}(T_p - T_b) = h_B(T_b - T_f) + H_b(T_b - T_a) \tag{3}$$

Where,

$$H_b = \frac{k_t}{l_t} \tag{4}$$

$$H_t = \left(\frac{1}{h_w + h_{rpa}}\right)^{-1} \tag{5}$$

$$h_{rpb} = \frac{\sigma(T_p + T_b)\left(T_p^2 + T_b^2\right)}{\left(\frac{1}{\varepsilon_p} + \frac{1}{\varepsilon_b} - 1\right)} \tag{6}$$

Fig. 3 Schematic representation of heat transfer characteristics across PVT air-collector

$$h_{rpb} = \varepsilon_p \sigma (T_p^2 + T_s^2)(T_p - T_s) \tag{7}$$

$$T_s = 0.0522 T_a^{1.5} \tag{8}$$

The equation for convective heat transfer coefficients was calculated according to the formula used by Fudholi et al. [35].

$$h = \frac{k}{D_c} N_u \tag{9}$$

$$D_c = \frac{4Wd}{2(W + d)} \tag{10}$$

The Nusselt number (N_u) depends on the Reynolds number (R_e) and can be calculated as:

Laminar flow region ($Re < 2300$)

$$N_u = 5.4 + \frac{0.00190 \left[Re \, Pr \left(\frac{D_c}{L} \right) \right]^{1.71}}{1 + 0.00563 \left[Re \, Pr \left(\frac{D_c}{L} \right) \right]^{1.17}} \tag{11}$$

Transition flow region ($2300 < Re < 6000$)

$$N_u = 0.116 (\overset{2/3}{Re} - 125) \overset{1/3}{Pr} \left[1 + \left(\frac{D_c}{L} \right)^{2/3} \right] \left(\frac{\mu}{\mu_w} \right)^{0.14} \tag{12}$$

Turbulent flow region ($Re > 6000$)

$$N_u = 0.018 \overset{0.8}{Re} \overset{0.4}{Pr} \tag{13}$$

Where Re and Pr are the Reynolds number and Prandtl number respectively and calculated as:

$$R_e = \frac{m D_c}{A_c \mu} \tag{14}$$

$$P_r = \frac{\mu C_f}{k} \tag{15}$$

The equations for physical properties of fluid circulated in the channel (air) is taken from Fudholi et al. [35]

$$\rho = 1.1774 - 0.00359(T - 27) \tag{16}$$

$$C_f = 1.0057 + 0.000066(T - 27) \tag{17}$$

$$k = 0.02624 + 0.0000758(T - 27) \tag{18}$$

$$\mu = [1.983 + 0.00184(T - 27)]10^{-5} \tag{19}$$

The temperature of the fluid (T_f) is the mean of inlet air temperature and outlet air temperature.

$$T_f = \frac{(T_{in} + T_{out})}{2} \tag{20}$$

To calculate the temperature vector, the Eq. (2)-(3) can be written in the form of a matrix

$$[A][T] = [B] \tag{21}$$

$$\begin{pmatrix} Z_1 & -Z_2 & -h_{rpb} \\ Z_4 & Z_5 & h_2 \\ h_{rpb} & h_2 & Z_7 \end{pmatrix} \begin{bmatrix} T_p \\ T_f \\ T_b \end{bmatrix} = \begin{bmatrix} Z_3 \\ Z_6 \\ Z_8 \end{bmatrix} \tag{22}$$

Where

$$Z_1 = H_t + h_A + h_{rpb} + (NA_n h_c \eta_n) \tag{23}$$

$$Q_t = NA_n h_c \eta_n (T_p - T_f) \tag{24}$$

$$Z_2 = h_A + (NA_n h_c \eta_n) = Z_4 \tag{25}$$

$$Z_3 = \tau \alpha I + H_t T_a - \eta_{pv} I \tag{26}$$

$$Z_5 = -[h_A + h_B + 2mC_f + (NA_n h_c \eta_n)] \tag{27}$$

$$Z_6 = -2mC_f T_{in} \tag{28}$$

$$Z_7 = -(h_B + h_{rpb} + H_b) \tag{29}$$

$$Z_8 = -H_b T_a \tag{30}$$

$$\eta_n = \frac{\tanh MH}{MH} \tag{31}$$

Where,

$$M = \left(\frac{2h_c}{k_n A_{cn}} \right)^{1/2} \tag{32}$$

$$h_A = h_B = h_c \tag{33}$$

At first, the heat transfer coefficients are estimated based on initial predicted values of temperature across various layers of PVT air-collector, i.e., ambient, air, PV, and backplate. The temperature vector is calculated according to Eq. (20).

$$[T] = [A]^{-1}[B] \tag{34}$$

The numerical values of designed parameters used in the study were: $L = 53.7$ cm, $W = 45.7$ cm, $\alpha = 0.9$, $\tau = 0.92$, $\epsilon_p = 0.7$, $\epsilon_b = 0.9$, $T_a = T_i = 27°C$ and $V_f = 1$ m/s. The temperature matrix obtained from Eq. (34) can be named as matrix $[T_1]$ and compared with the initial predicted values of temperature [T]. The value of the iteration is set by comparing the previous matrix with a new matrix. If the difference between the two sets of values is lower than 0.001, then the iteration stops, and the old temperature values are changed by new values of T_a, T_f, T_p, and T_b. The iterative process used to obtain the theoretical results has been shown in Fig. 4. Further, it has been observed that adequate convergence for the temperatures was accomplished in three to four iterations.

Fig. 4 Flowchart representing the process of theoretical solution
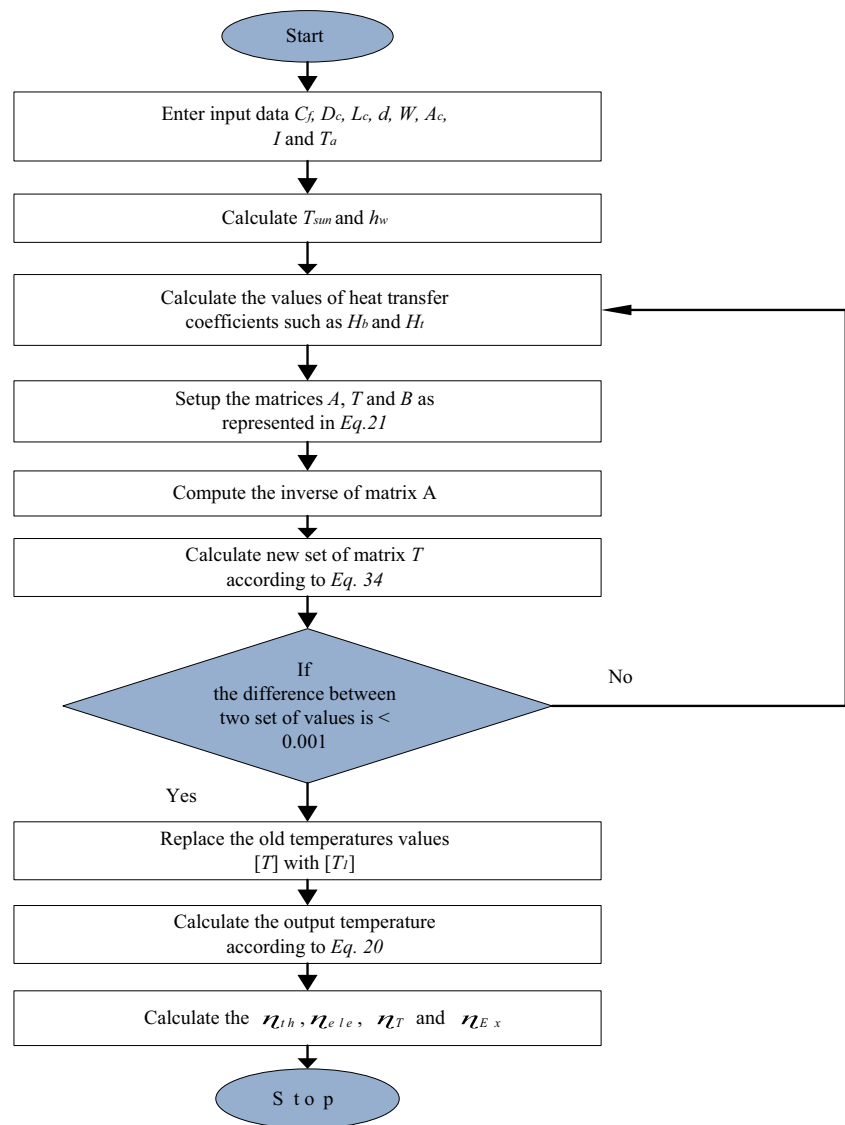
2.1 Performance parameters of PVT air-collector

The performance of the PVT air-collector is measured in the form of electrical (η_{ele}), thermal (η_{th}), and exergy efficiency (η_{Ex}). The overall efficiency of the PVT is the aggregate of electrical and thermal efficiencies [36]

$$\eta_{overall} = \eta_{th} + \eta_{ele} \qquad (35)$$

The η_{th} of the PVT-collector is written as

$$\eta_{th} = \frac{Q_t}{IA_c} \qquad (36)$$

Where Q_t is the collected heat, which may be written as

$$Q_t = mC_f(T_o - T_i) \qquad (37)$$

The η_{ele} of PVT air-collector depends upon the temperature of the solar cell, temperature coefficient of efficiency, and the ambient temperature

$$\eta_{ele} = \eta_0[1 - \beta_0(T_{cell} - T_a)] \qquad (38)$$

Apart from these, exergy efficiency (η_{Ex}) is also taken as a parameter for evaluating the efficiency of the PVT-system as it helps in reducing the inefficiencies of the system [37].

$$\eta_{Ex} = \frac{Ex_{out}}{Ex_{in}} \times 100 \qquad (39)$$

The exergy balance in a PVT air-collector is calculated according to Das et al. [30].

$$Ex_{out} = \sum Ex_{th} + \sum Ex_{el} \qquad (40)$$

Where,

$$\sum Ex_{th} = Q_t - mC_f T_a \ln \frac{T_o}{T_i} \qquad (41)$$

$$\sum Ex_{el} = \left[\frac{\eta I A_c}{1000} \right] \qquad (42)$$

The input exergy is calculated according to the relation presented by Kalogirou et al. [38]

$$\sum Ex_{in} = A_c N_c I \left[1 - \left(\frac{4}{3} \right) \left[\frac{T_a}{T_{sun}} \right] + \left(\frac{1}{3} \right) \left[\frac{T_a^4}{T_{sun}^4} \right] \right] \qquad (43)$$

3 Methodology

3.1 Study area

The experimental study is conducted in Ghaziabad City, India, with the coordinates of 28.667856° N and 77.4538° E. It resides close-in location and latitude to New Delhi. The climatic conditions of Ghaziabad are similar to the national capital of New Delhi. The estimated ambient temperature ranges between 21 and 40°C, with an average wind speed of 2.4 m/s and approximate humidity of 67.7%. The city receives its maximum rainfall in July and August, with an average of 236.2 mm of precipitation. The approximated hour of sunshine ranging between 200 and 300 h. Since the city receives good sunshine hours throughout the year, steady growth in solar photovoltaic projects has been observed in the last decade. The climatic conditions are favorable for performing the experimental investigation on PVT technology.

3.2 PVT air-collector description

Figure 5 represents the schematic of the experimental set-up of PVT air-collector with the V-groove absorber in the channel. The experimental set-up consists of a PV-module, V-groove, low power brushless DC fan, and data acquisition unit to record the observations. The PV-module employed in the fabrication of PVT air-collector was developed by Central Electronics Limited (CEL) India. The size of the module is 537*457*35 mm with open-circuit voltage and short circuit current of 21.8 V and 2.74 A, respectively. The other specifications of the PV- module are mentioned in Table 3.

The V-groove used in the channel of the PVT air-collector works as an absorber and installed at the backside of the 40 W PV-panel. The length, vertex angle, and height of each side of the individual groove is 53.2 cm, 60°, and 3.5 cm, respectively. Thermal grease was used to fix the V-groove in the channel to avoid the heat loss into the surroundings. Experiments were

performed on 7th June 2019 for the climatic condition of Ghaziabad, India.

3.3 Measuring instruments

The solar radiations were measured using a class 2 pyranometer; A J-type thermocouple was employed to estimate the temperature across the various layers. The solar radiations and ambient temperature are recorded at 30 minutes interval, and the experiment performed between 07:00 a.m. to 5:30 p.m. An anemometer (PCE-VA 11) is employed to estimate the air velocity at the inlet and outlet of the channel. The measuring instruments used for the experiment are specified in Table 4.

3.4 Uncertainty analysis

To ensure accurate results and avoid errors in the measurement, it is essential to conduct the uncertainty analysis. During experiments, while measuring air velocity, temperature, and sunlight intensity, specific errors and uncertainties can occur in the results due to the selections of the instrument, calibration, handling of instruments, and recordings. These uncertainties may slightly alter the experimental results from the theoretical results obtained from mathematical modeling. The uncertainties can be estimated by using the relation:

$$X_R = \left[(x_1)^2 + (x_2)^2 + (x_3)^2 + \cdots \cdots + (x_n)^2 \right]^{1/2} \qquad (44)$$

Where,
X_R is the uncertainty in the experimental result.
$x_1, x_2, \ldots \ldots x_n =$ Uncertainties in the individual variables.
The error analysis (e) was performed to validate experimental and theoretical models.

$$e = \sqrt{\frac{\sum (e_i)^2}{N}} \qquad (45)$$

Where,

$$e_i = \left(\frac{x_i - y_i}{x_i} \right) \times 100 \qquad (46)$$

X_i, Y_i are the theoretical and experimental figures of the variable.
The accuracy among the theoretical and experimental outcomes was measured according to Eq. (45).

4 Results and discussion

In this paper, the performance of PVT air-collector with low-cost V-groove absorber in the channel is experimentally as

Fig. 5 Schematic diagram of the Experimental set-up of PVT air-collector with V-groove absorber
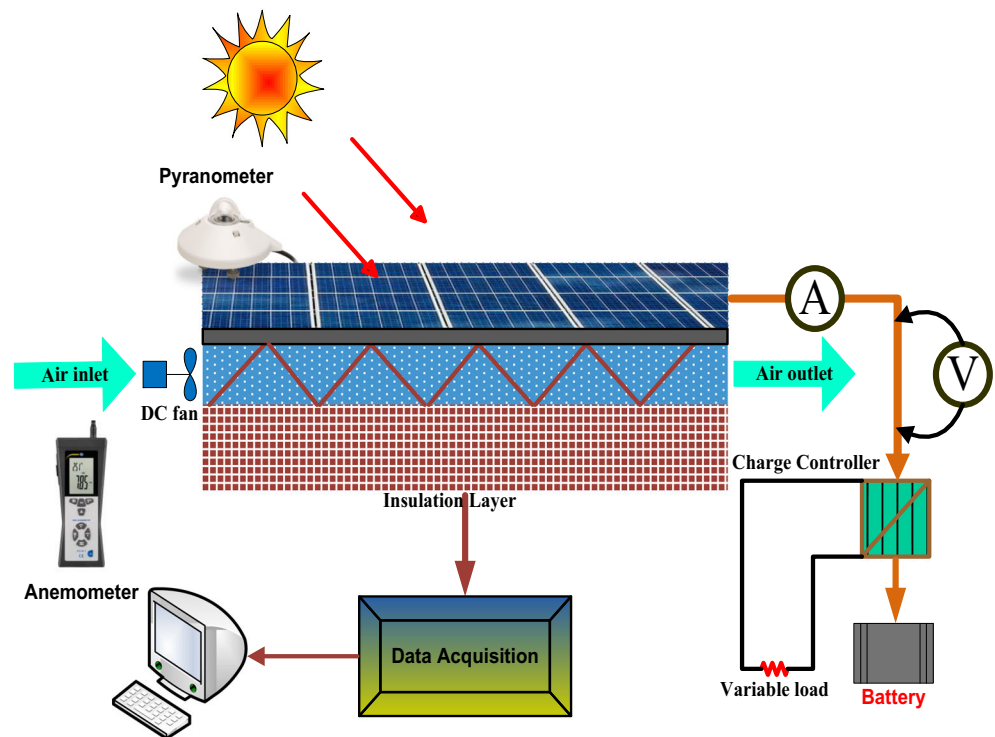
well as theoretically investigated for the climate of Ghaziabad City (28.667856° N, 77.4538° E), India in June 2019. To justify its applicability and acceptability, various parameters such as η_{ele}, η_{th}, $\eta_{overall}$, and η_{Ex} have been calculated for the proposed model. A mathematical model is formulated to predict the thermal and electrical efficiencies of the proposed system, and the outcomes are verified with the experimental results. The parameter of proposed PVT-setup, such as solar radiations (W/m2), ambient temperature, fluid temperature, and inlet-outlet temperatures of the channel has been measured regularly at an interval of 30 minutes. Therefore, the analysis of experimental observations relied on a half-hour average measurement.

The deviation in climatic parameters, viz. global solar radiations, and ambient temperature during 07:00 a.m. to 5:30 p.m. for a day in June 2019 is shown in Fig. 6. The data for

solar radiations and ambient temperature is recorded for a particular day (7th June 2019) at an interval of 30 minutes.

As demonstrated in Fig. 6, the ambient temperature (T_a) increases with time. The average T_a is 35.40°C. The solar radiation is maximum at around 12:30 p.m., which is 907 W/m². The PV-cell temperature is an important parameter that directly affects the performance of PV-systems. It has been mentioned that the electrical efficiency (η_{ele}) of the PV-system decreases on the rise in temperature of cells [37]. Therefore, it is always essential to keep the cell temperature within limits. Figure 7 shows the hourly variation of η_{ele} with time on 7th June 2019. It has been observed from the figure that a reasonable value of η_{ele} is obtained, although the conditions are not very favorable. The proper functioning of the channel below the PV-module ensures that the rise in PV-cell temperature is not very high and still within the acceptable limits. A noticeable decrement in η_{ele} is observed from 3:00 p.m. to 4:00 p.m., and during that particular period, the cell temperature reached its highest value.

It has been observed that the average η_{ele} is 10.39% and 10.26% for theoretical and experimental analysis. Hence, the theoretical results are coherent with experimental results with an accuracy of 98.8%, as illustrated in Table 5.

Figure 8 provides a comparison of PV, outlet, and inlet temperatures obtained from both the theoretical and experimental models. It has been observed that the theoretical results obtained using the mathematical model were coherent with experimental results obtained in real outdoor conditions with an accuracy of greater than 90% in each case.

Table 3 PV-module Specifications

Specification	Value
Current at P_{max}	2.20A
Dimensions of the channel	537*457*35 mm
Nominal Power (P_{max})	40Wp
Open circuit voltage (V_{oc})	21.8 V
Short circuit current (I_{sc})	2.74 A
Temperature coefficient of eff. (β_0)	0.004
Type	Polycrystalline

Table 4 List of instruments used for measurement

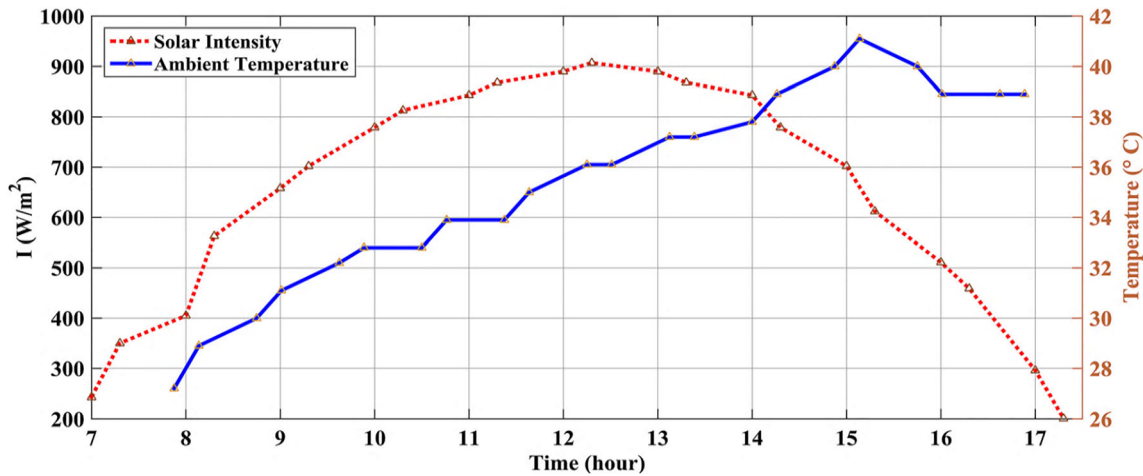| Instrument	Measured parameter	Type	Operating range	Accuracy
Thermocouple	Upper surface temperature	Type J	-210°C to 760°C	0.4%
Anemometer	Air velocity	PCE-VA 11	0.4 m/s to 30 m/s	± 3%
Pyranometer	Intensity	Class 2	0-2000W/m^2	5%
Multi-meter	Voltage and current	Digital	(0-600volt) AC/DC	0.8%
			(0-10A) AC/DC	

Fig. 6 Global solar radiations and ambient temperature on an hourly basis

The thermal efficiency (η_{th}) of the PVT-system depends upon the temperature difference between the PVT-collector output and input (T_0-T_i), as mentioned in Eq. (36)-(37). T_0-T_i also indicates that temperature in the PVT-collector is successfully absorbed by the air. Figure 9 shows the deviation of η_{th} with the temperature difference between the input-output of the collector. It has been observed that the η_{th} is high when an appreciable temperature difference T_0-T_i is obtained.

Table 6 depicts the theoretical calculation of temperatures along with thermal efficiency variations. The average η_{th} is

41.78% and 41.57% for theoretical and experimental studies, respectively. The mathematical modeling results are coherent with the experimental results with an accuracy of 99.43%.

Figure 10 shows the hourly variation of overall efficiency ($\eta_{overall}$) obtained both theoretically and experimentally.

The average value of $\eta_{overall}$ obtained for the theoretical and experimental model were 52.21% and 51.88%, respectively. Further, it has been observed that the accuracy between both models is greater than 95%. It is noticed that minimal variation is observed in $\eta_{overall}$ as compared to thermal and
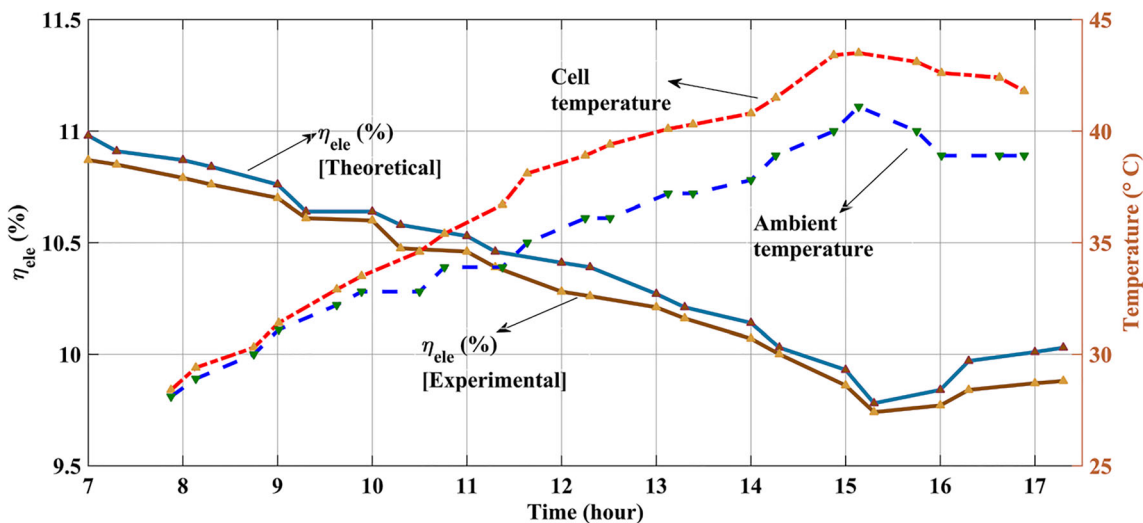

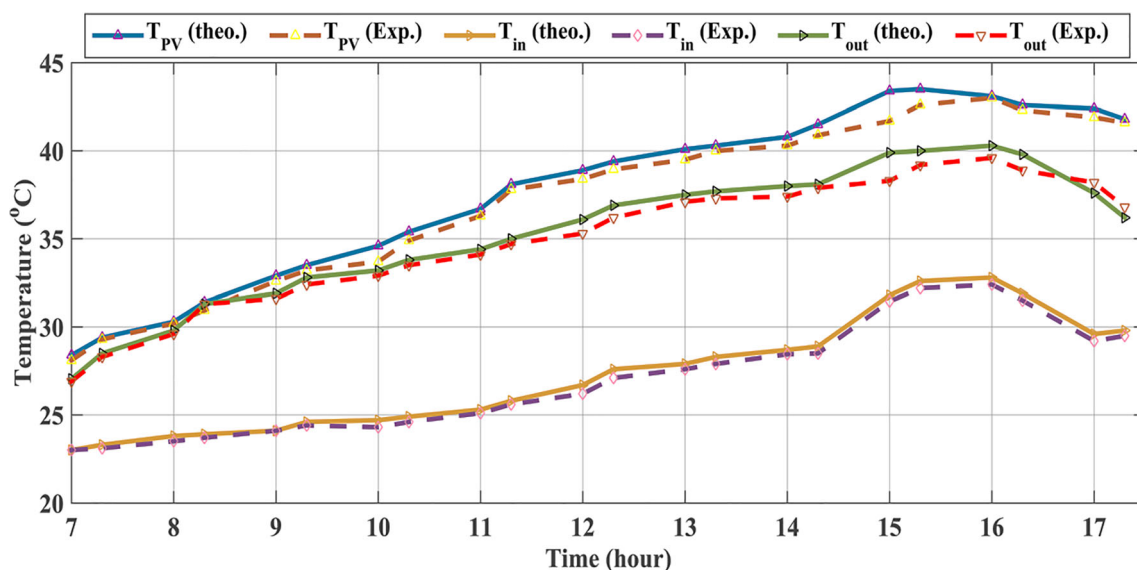**Fig. 7** Electrical efficiency variation with temperature

Table 5 Comparison of theoretical and experimental results for electrical efficiency

Time	Solar Intensity (W/m^2)	Ambient temperature (^{o}C)	Electrical efficiency (%) (Theoretical)	Electrical efficiency (%) (Experimental)	Error (%)
7:00	243	27.2	10.99	10.85	1.29
7:30	350	28.9	10.91	10.80	1.01
8:00	405	30.0	10.87	10.76	1.01
8:30	563	31.1	10.84	10.72	1.11
9:00	658	32.2	10.76	10.68	0.75
9:30	702	32.8	10.67	10.56	1.03
10:00	779	32.8	10.64	10.49	1.41
10:30	813	33.9	10.58	10.43	1.42
11:00	843	33.9	10.55	10.42	1.23
11:30	868	35.0	10.46	10.36	0.97
12:00	890	36.1	10.43	10.25	1.73
12:30	907	36.1	10.39	10.21	1.25
13:00	890	37.2	10.27	10.17	0.98
13:30	868	37.2	10.24	10.14	0.99
14:00	843	37.8	10.18	10.07	1.01
14:30	779	38.9	10.03	09.96	0.70
15:00	702	40.0	09.93	09.86	0.71
15:30	612	41.1	09.82	09.74	0.82
16:00	511	40.0	09.84	09.76	0.81
16:30	459	38.9	09.97	09.81	1.61
17:00	296	38.9	10.03	09.83	1.99
17:30	201	38.9	10.06	09.85	2.09
Average error			10.39	10.26	1.18

electrical efficiencies because of the compensating effect of one parameter over the other. i.e., when one parameter shows increasing behaviour, the other shows decreasing behaviour.

The electric power output from the experimental set-up varies linearly with solar radiation. Based on the analysis, the maximum electrical power obtained from the experimental set-up is 37.96 W, obtained when the intensity is 890 W/m^2. Figure 11 demonstrate the deviation in voltage and current of the proposed experimental set-up. It is evident that the voltage of the PV-collector drops sharply with the rise in solar

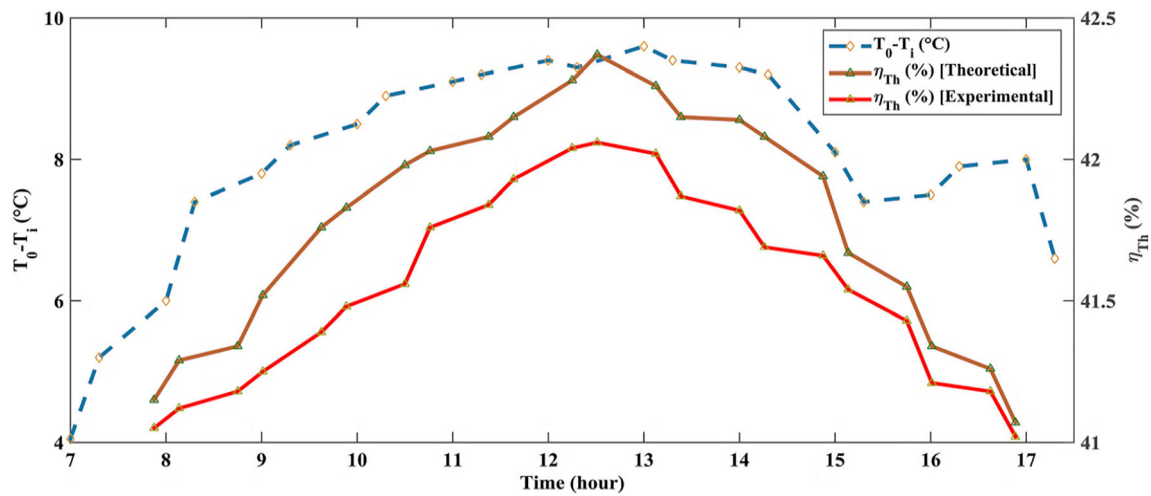**Fig. 8** Theoretical and experimental variation of temperature

Fig. 9 Thermal efficiency variation with temperature difference

radiation and PV temperature. The numerical value of V_{oc} and I_{max} obtained from the experimental set-up were 19.62V and 2.25A, respectively.

The thermal and electrical efficiencies are not the only performance parameters for hybrid PVT- systems; an exergy analysis is also performed to evaluate the overall efficiency of the system. The exergy efficiency is evaluated by calculating the thermal and electrical exergies separately. Figure 12 shows the exergy efficiency (η_{Ex}) of the PVT-system with V-groove in the channel evaluated both theoretically and experimentally.

The average η_{Ex} of the PVT air-collector with V-groove absorber is 12.94% and 12.70% for theoretical and experimental studies, respectively, as shown in Table 7. It has been

Table 6 Experimental and theoretical variation of thermal efficiency

| Time	Temperature (°C)					Thermal efficiency (%η_{th})		
	T_a	T_{cell}	T_i	T_o	$T_o - T_i$	Theoretical	Experimental	Error
7:00	27.2	28.4	23.0	27.05	4.05	41.15	41.05	0.243
7:30	28.9	29.4	23.3	28.5	5.2	41.29	41.12	0.411
8:00	30.0	30.3	23.8	29.8	6.0	41.34	41.18	0.387
8:30	31.1	31.4	23.9	31.3	7.4	41.52	41.25	0.650
9:00	32.2	32.9	24.1	31.9	7.8	41.76	41.39	0.886
9:30	32.8	33.5	24.6	32.8	8.2	41.83	41.48	0.836
10:00	32.8	34.6	24.7	33.2	8.5	41.98	41.56	1.000
10:30	33.9	35.4	24.9	33.8	8.9	42.03	41.76	0.642
11:00	33.9	36.7	25.3	34.4	9.1	42.08	41.84	0.570
11:30	35.0	38.1	25.8	35.0	9.2	42.15	41.93	0.521
12:00	36.1	38.9	26.7	36.1	9.4	42.28	42.04	0.567
12:30	36.1	39.4	27.6	36.9	9.3	42.37	42.06	0.731
13:00	37.2	40.1	27.9	37.5	9.6	42.26	42.02	0.567
13:30	37.2	40.3	28.3	37.7	9.4	42.15	41.87	0.664
14:00	37.8	40.8	28.7	38.0	9.3	42.14	41.82	0.760
14:30	38.9	41.5	28.9	38.1	9.2	42.08	41.69	0.926
15:00	40.0	43.4	31.8	39.9	8.1	41.94	41.66	0.667
15:30	41.1	43.5	32.6	40.0	7.4	41.67	41.54	0.320
16:00	40.0	43.1	32.8	40.3	7.5	41.55	41.43	0.288
16:30	38.9	42.6	31.9	39.8	7.9	41.34	41.21	0.314
17:00	38.9	42.4	29.6	37.6	8.0	41.26	41.18	0.194
17:30	38.9	41.8	29.8	36.2	6.6	41.07	41.00	0.122
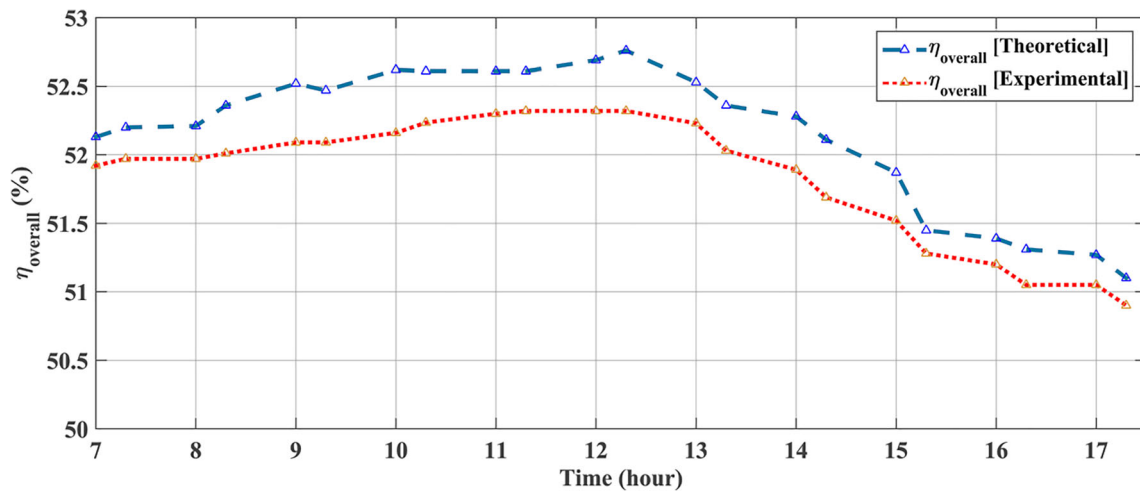
Fig. 10 Variation in overall efficiency with time
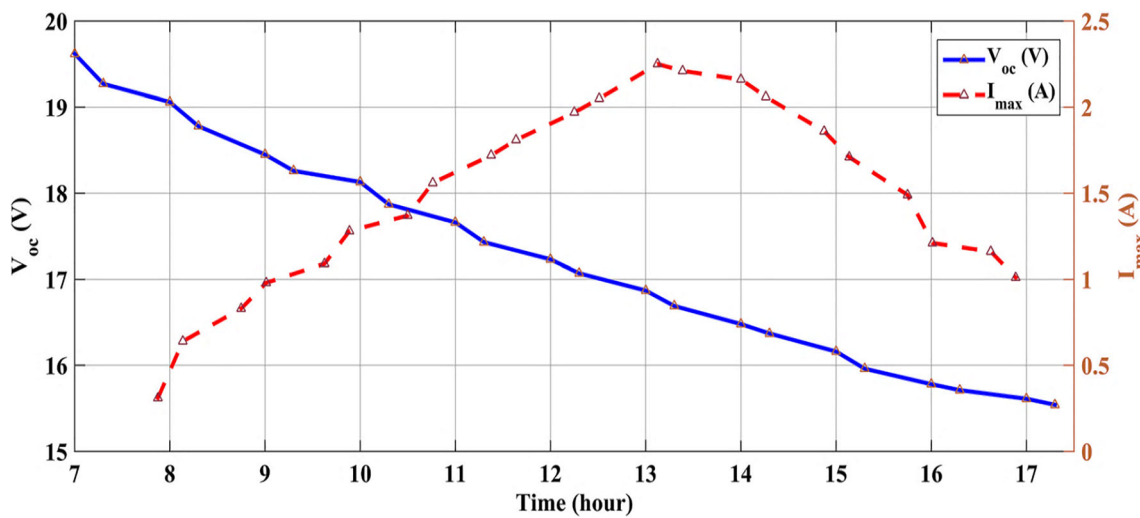

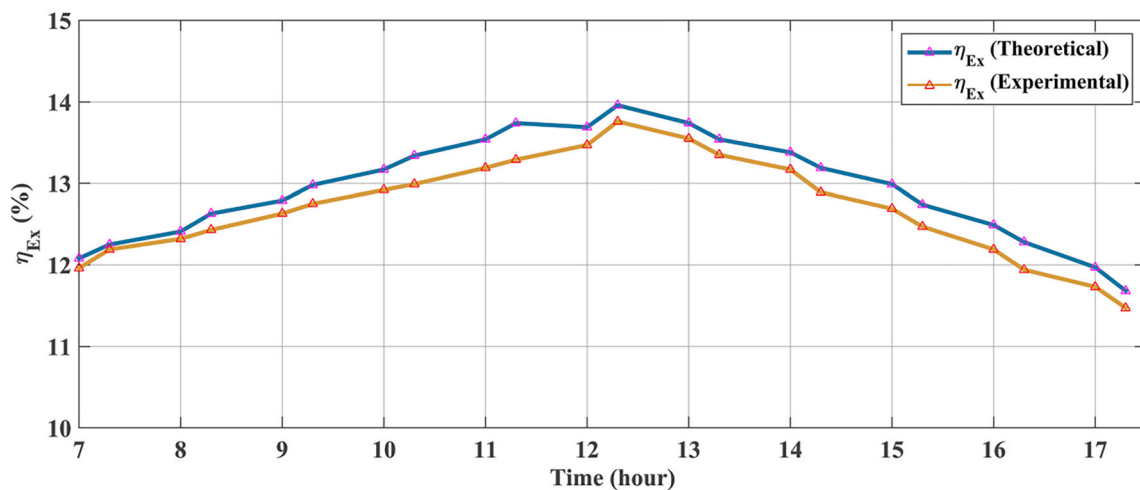**Fig. 11** Voltage and current variation of PV-collector with time

Fig. 12 Exergy efficiency variation with time

Table 7 Theoretical and experimental results of exergy efficiency

Time	Solar Intensity (W/m^2)	Ambient temperature (^{o}C)	Exergy efficiency (%) (Theoretical)	Exergy efficiency (%) (Experimental)	Error (%)
7:00	243	27.2	12.08	11.96	0.99
7:30	350	28.9	12.25	12.19	0.49
8:00	405	30.0	12.41	12.32	0.73
8:30	563	31.1	12.63	12.43	1.59
9:00	658	32.2	12.79	12.63	1.25
9:30	702	32.8	12.98	12.75	1.78
10:00	779	32.8	13.17	12.92	1.90
10:30	813	33.9	13.34	12.99	2.62
11:00	843	33.9	13.54	13.19	2.59
11:30	868	35.0	13.74	13.29	3.28
12:00	890	36.1	13.69	13.47	1.60
12:30	907	36.1	13.96	13.76	1.43
13:00	890	37.2	13.74	13.55	1.38
13:30	868	37.2	13.54	13.35	1.40
14:00	843	37.8	13.38	13.17	1.56
14:30	779	38.9	13.19	12.89	2.28
15:00	702	40.0	12.99	12.69	2.31
15:30	612	41.1	12.74	12.47	2.12
16:00	511	40.0	12.49	12.19	2.40
16:30	459	38.9	12.28	11.94	2.77
17:00	296	38.9	11.97	11.73	2.01
17:30	201	38.9	11.68	11.47	1.80
Average error			12.94	12.70	1.83

concluded that the results obtained using mathematical modeling were coherent with the experimental results obtained in real outdoor conditions with an accuracy of approximately 98.17%.

5 Conclusion

In this paper, a PVT air-collector is designed with V-groove in the air channel and investigated experimentally in real outdoor conditions with detailed mathematical modeling. The manuscript is best concluded as:

- A matrix-inversion method has been adopted to solve the temperature equations.
- Mathematical model results are validated with the experimental results with the help of error analysis.
- The average overall efficiency of the proposed system is 52.21% and 51.88% for theoretical and experimental studies, respectively.
- The theoretical and experimental values of exergy efficiency are 12.94% and 12.70%, respectively, with an accuracy of 98.17%.
- A significant improvement has been observed in the energy and exergy efficiencies of the PV-panel using the proposed set-up.

- The temperature of the PV-cell was highest among all other components of the PVT-setup. Also, the overall efficiency and exergy efficiency is maximum on optimum solar intensity.
- The thermal efficiency of the proposed system is 41.78% and 41.57% for theoretical and experimental studies, respectively.
- The overall efficiency of the proposed PVT-system has been considerably improved with the V-groove in the channel.

Compliance with ethical standards

References

1. (2019) Mercom India Research: clean energy news and insights, vol 01, issue 02
2. Bridge to India (n.d.) Available: https://bridgetoindia.com/backend/wp-content/uploads/2019/12/India-Solar-Rooftop-map-Sep-2019.pdf
3. Tomar V, Tiwari G, Bhatti TS, Norton B (2018) Thermal modeling and experimental evaluation of five different photovoltaic modules

integrated on prototype test cells with and without water flow. Energy Convers Manag 165:219–235

4. Yamawaki T, Mizukami S, Masui T, Takahashi H (2001) Experimental investigation on generated power of amorphous PV module for roof azimuth. Solar Energy Mater Solar Cells 67:369–377

5. Norton B, Eames PC, Mallick TC, Huang MJ, McCormack SJ, Mondol JD, Yigzaw GY (2011) Enhancing the performance of building integrated photovoltaic. Sol Energy 85(8):1629–1664

6. Kern EC Jr, Russell MC (1978) Combined photovoltaic and thermal hybrid collector systems. In: Proceedings of the 13th IEEE photovoltaic specialists. Washington, DC, pp 1153–7

7. Diwania S, Agrawal S, Siddiqui AS (2018) Performance enhancement of single-channel glazed photovoltaic thermal module using Whale Optimisation Algorithm and its comparative study. Int J Ambient Energy. https://doi.org/10.1080/01430750.2018.1537937

8. Tian Y, Zhao CY (2013) A review of solar collectors and thermal energy storage in solar thermal applications. Appl Energy 104:538–553

9. Kazemian A, Hosseinzadeh M, Sardarabadi M, Passandideh-Fard M (2018) Effect of glass cover and working fluid on the performance of photovoltaic thermal (PVT) systems. An experimental study. Sol Energy 173:1002–1010

10. Lammle M, Kroyer T, Fortuin S, Wiese M, Hermann M (2016) Development and modeling of highly-efficient PVT collectors with low-emissivity coatings. Sol Energy 130:161–173

11. Rejeb O, Dhaou H, Jemni A (2015) A numerical investigation of a photovoltaic thermal (PV/T) collector. Renew Energy 77:43–50

12. Yazdanifard F, Ebrahimnia-Bajestan E, Ameri M (2016) Investigating the performance of a water-based photovoltaic/thermal (PV/T) collector in laminar and turbulent flow regime. Renew Energy 99:295–306

13. Abbas N, Awan MB, Amer M, Ammar SM, Sajjad U, Ali HM, … Jafry AT (2019) Applications of nano-fluids in photovoltaic thermal systems: A review of recent advances. Statistical Mechanics and Its Applications, Physica A, p 122513

14. Sardarabadi M, Hosseinzadeh M, Kazemian A, Passandideh-Fard M (2017) Experimental investigation of the effects of using metal-oxides/water nano-fluids on a photovoltaic thermal system (PVT) from energy and exergy viewpoints. Energy 138:682–695

15. Ali H, Miqdam T, Hussein A, Abdulrasool H, Najah A (2017) An experimental investigation of SiC nano-fluid as a base-fluid for a photovoltaic thermal PV/T system. Energy Convers Manag 142:547–58

16. Singh PH, Jain A, Singh A, Arora S (2019) Influence of absorber plate shape factor and mass flow rate on the performance of the PVT system. Appl Therm Eng. https://doi.org/10.1016/j.applthermaleng.2019.04.070

17. Jones D, Lammle M, Theis D, Schneider S, Fray G (2019) Performance modeling of PVT collectors: Implementation, validation, and parameter identification approach using TRANSYS. Sol Energy 193:51–64

18. Fudholi A, Zohri M, Rukman NSB, Nazri NS, Mustapha M, Yen CH, Sopian K (2019) Exergy and sustainability index of photovoltaic thermal (PVT) air collector: A theoretical and experimental study. Renew Sustain Energy Rev 100:44–51

19. Salem MR, Ali RK, Elshazly KM (2017) Experimental investigation of the performance of a hybrid photovoltaic/thermal solar system using aluminium cooling plate with straight and helical channels. Sol Energy 157:147–156

20. Tadesse M (2017) Design, modeling, and performance analysis of parallel flow double pass V-groove solar air collector for preservation of onion in university students' cafeteria: Wolaita Sodo University. Int J Recent Dev Eng Technol 6(6):1–12

21. Khanjari Y, Pourfayaz F, Kasaeian AB (2016) Numerical investigation on using of nanofluid in a water-cooled photovoltaic thermal system. Energy Convers Manag 122:263–278

22. Hazami M, Riahi A, Mehdaoui F, Nouicer O, Farhat A (2016) Energetic and exergetic performances analysis of a PV/T (photovoltaic thermal) solar system tested and simulated under to Tunisian (North Africa) climatic conditions. Energy 107:78–94

23. Jahromi SN, Vadiee A, Yaghoubi M (2015) Exergy and economic evaluation of a commercially available PV/T collector for different climates in Iran. Energy Proc 75:444–56

24. Ibrahim A, Fudholi A, Sopian K, Othman MY, Ruslan MH (2014) Efficiencies and improvement potential of building integrated photovoltaic thermal (BIPVT) system. Energy Convers Manag 77:527–534

25. Gholampour M, Ameri M (2016) Energy and exergy analyses of Photovoltaic/Thermal flat transpired collectors: experimental and theoretical study. Appl Energy 164:837–856

26. Wu SY, Zhang QL, Xiao L, Guo FH (2011) A heat pipe photovoltaic/thermal (PV/T) hybrid system and its performance evaluation. Energy Build 43:3558–3567

27. Sarhaddi F, Farahat S, Ajam H, Behzadmehr A (2010) Exergetic performance assessment of a solar photovoltaic thermal (PV/T) air collector. Energy Build 42:2184–2199

28. Khaki M, Shahsavar A, Khanmohammadi S, Salmanzadeh M (2017) Energy and exergy analysis and multi-objective optimization of an air based building integrated photovoltaic/thermal (BIPV/T) system. Sol Energy 158:380–395

29. Agrawal B, Tiwari GN (2010) Optimizing the energy and exergy of building integrated photovoltaic thermal (BIPVT) systems under cold climatic conditions. Appl Energy 87:417–426

30. Das D, Kalita P, Roy O (2018) Flat plate hybrid photovoltaic-thermal (PV/T) system: a review on design and development. Renew Sustain Energy Rev 84:111–130

31. Said SAM, Walwil HM (2014) Fundamental studies on dust fouling effects on PV module performance. Sol Energy 107:328–337

32. Gupta V, Sharma M, Pauchari RK, Dinesh Babu KN (2019) Comprehensive review on effect of dust on solar photovoltaic system and mitigation techniques. Sol Energy 191:596–622

33. Molki A (2010) Dust affects solar-cell efficiency. Phys Educ 45:456–458

34. Kazem HA, Khatib T, Sopian K (2013) Effect of dust deposition on the performance of multi-crystalline photovoltaic modules based on experimental measurements. Renew Energy 3:850–853

35. Fudholi A, Zohri M, Jin G, Ibrahim A, Yen CH, Othman MY, Ruslan MH, Sopian K (2018) Energy and exergy analysis of photovoltaic thermal collector with ∇-groove. Sol Energy 159:742–750

36. Diwania S, Agarwal S, Siddiqui AS, Singh S (2020) Photovoltaic–thermal (PV/T) technology: a comprehensive review on applications and its advancement. Int J Energy Environ Eng 11:33–54

37. Petela R (2003) Exergy of undiluted thermal radiation. Sol Energy 74(6):469–488

38. Kalogirou SA, Sotirios K, Konstantinos B, Camelia S, Badescu V (2016) Exergy energy of solar thermal collectors and processes. Prog Energy Combust Sci 56:106–137